In vivo and *in situ* cellular imaging full-field optical coherence tomography with a rigid endoscopic probe

Anne Latrive[1,2,*] and A. Claude Boccara[1,2]

[1]*Institut Langevin, ESPCI-ParisTech, 10 rue Vauquelin, 75005 Paris, France*
[2]*LLTech, 6 place de la Madeleine, 75008 Paris, France*
**anne.latrive@espci.fr*

Abstract: Full-field OCT has proved to be a powerful high-resolution cellular imaging tool for biological tissues. However the standard bulk full-field OCT setup does not match the size requirements for most *in situ* and *in vivo* imaging applications. We adapted its principle into a rigid needle-like probe using two coupled interferometers and incoherent illumination: an external processing interferometer is used for in-depth scanning, while a distal common-path interferometer at the tip of the probe collects light backscattered from the tissue. Our experimental setup achieves an axial and transversal resolution in tissue of 1.8 µm and 3.5 µm respectively, for a sensitivity of −80 dB. We present *ex vivo* images of human breast tissue, and *in vivo* images of different areas of human skin, which reveal cellular-level structures.

OCIS codes: (180.3170) Interference microscopy; (110.4500) Optical coherence tomography; (110.2760) Gradient-index lenses; (170.2150) Endoscopic imaging; (170.3880) Medical and biological imaging

References and links

1. D. Huang, E. A. Swanson, C. P. Lin, J. S. Schuman, W. G. Stinson, W. Chang, M. R. Hee, T. Flotte, K. Gregory, C. A. Puliafito, and J. G. Fujimoto, "Optical coherence tomography," Science **254**(5035), 1178–1181 (1991).
2. G. J. Tearney, M. E. Brezinski, B. E. Bouma, S. A. Boppart, C. Pitris, J. F. Southern, and J. G. Fujimoto, "*In vivo* endoscopic optical biopsy with optical coherence tomography," Science **276**(5321), 2037–2039 (1997).
3. T. P. M. Goderie, G. van Soest, H. M. Garcia-Garcia, N. Gonzalo, S. Koljenović, G. J. L. H. van Leenders, F. Mastik, E. Regar, J. W. Oosterhuis, P. W. Serruys, and A. F. W. van der Steen, "Combined optical coherence tomography and intravascular ultrasound radio frequency data analysis for plaque characterization. Classification accuracy of human coronary plaques *in vitro*," Int. J. Cardiovasc. Imaging **26**(8), 843–850 (2010).
4. N. V. Iftimia, M. Mujat, T. Ustun, R. D. Ferguson, V. Danthu, and D. X. Hammer, "Spectral-domain low coherence interferometry/optical coherence tomography system for fine needle breast biopsy guidance," Rev. Sci. Instrum. **80**(2), 024302 (2009).
5. B. C. Quirk, R. A. McLaughlin, A. Curatolo, R. W. Kirk, P. B. Noble, and D. D. Sampson, "*In situ* imaging of lung alveoli with an optical coherence tomography needle probe," J. Biomed. Opt. **16**(3), 036009 (2011).
6. D. Sacchet, J. Moreau, P. Georges, and A. Dubois, "Simultaneous dual-band ultra-high resolution full-field optical coherence tomography," Opt. Express **16**(24), 19434–19446 (2008).
7. M. Jain, N. Shukla, M. Manzoor, S. Nadolny, and S. Mukherjee, "Modified full-field optical coherence tomography: A novel tool for rapid histology of tissues," J Pathol Inform **2**(28), 28 (2011).
8. O. Assayag, A. Latrive, M. Antoine, B. Sigal, A. Burcheri, F. Harms, B. de Poly, S. Gigan, and A. C. Boccara, "*Ex situ* and *in situ* intra-operative optical biopsy using Light-CT," presented at Advances in Optics for Biotechnology, Medicine and Surgery XII, Naples, Florida, USA, June 5–8, 2011 (Engineering Conferences International).
9. W.-Y. Oh, B. E. Bouma, N. Iftimia, R. Yelin, and G. J. Tearney, "Spectrally-modulated full-field optical coherence microscopy for ultrahigh-resolution endoscopic imaging," Opt. Express **14**(19), 8675–8684 (2006).
10. H. D. Ford and R. P. Tatam, "Fibre imaging bundles for full-field optical coherence tomography," Meas. Sci. Technol. **18**(9), 2949–2957 (2007).
11. H. D. Ford, R. Beddows, P. Casaubieilh, and R. P. Tatam, "Comparative signal-to-noise analysis of fibre-optic based optical coherence tomography systems," J. Mod. Opt. **52**(14), 1965–1979 (2005).

#150895 - $15.00 USD Received 11 Jul 2011; accepted 23 Jul 2011; published 29 Sep 2011

12. A. Dubois and A. C. Boccara, "Full-field optical coherence tomography" in *Optical Coherence Tomography*, E.D. W. Drexler and J. G. Fujimoto, eds. (Springer, 2009), pp. 565–591.
13. H. D. Ford and R. P. Tatam, "Full-field optical coherence tomography using a fibre imaging bundle," Proc. SPIE **6079**, 60791H (2006).
14. P. H. Tran, D. S. Mukai, M. Brenner, and Z. Chen, "*In vivo* endoscopic optical coherence tomography by use of a rotational microelectromechanical system probe," Opt. Lett. **29**(11), 1236–1238 (2004).
15. L. Vabre, A. Dubois, and A. C. Boccara, "Thermal-light full-field optical coherence tomography," Opt. Lett. **27**(7), 530–532 (2002).
16. P. J. Dwyer, C. A. DiMarzio, and M. Rajadhyaksha, "Confocal theta line-scanning microscope for imaging human tissues," Appl. Opt. **46**(10), 1843–1851 (2007).
17. A. D. Aguirre, J. Sawinski, S.-W. Huang, C. Zhou, W. Denk, and J. G. Fujimoto, "High speed optical coherence microscopy with autofocus adjustment and a miniaturized endoscopic imaging probe," Opt. Express **18**(5), 4222–4239 (2010).
18. H. Zhong, Z. Guo, H. Wei, C. Zeng, H. Xiong, Y. He, and S. Liu, "In vitro study of ultrasound and different-concentration glycerol-induced changes in human skin optical attenuation assessed with optical coherence tomography," J. Biomed. Opt. **15**(3), 036012 (2010).
19. T. Xie, S. Guo, Z. Chen, D. Mukai, and M. Brenner, "GRIN lens rod based probe for endoscopic spectral domain optical coherence tomography with fast dynamic focus tracking," Opt. Express **14**(8), 3238–3246 (2006).

1. Introduction

Since its beginning in the early nineties [1], Optical Coherence Tomography (OCT) has proven its interest for many biomedical fields thanks to its virtual slicing and 3D imaging capability. The most important domain of application is still ophthalmology, where its ability to differentiate between layers of the retina has made it a standard diagnosis procedure. The adaptation of the OCT technique into endoscopic setups [2] allows the access to a variety of areas of the human body where high resolution in-depth imaging is needed. Endoscopic OCT is now mainly used for intravascular imaging [3] where it is able to distinguish between different types of plaques. A second main domain of application is biopsy guidance with needle-like probes [4,5]. However the typical axial and transversal resolutions of such OCT systems lie between 5 and 30 µm, which is not enough to distinguish cellular-scale structures.

Full-field OCT (FFOCT) is a particular approach of OCT which directly takes "en face" 2-D images with an isotropic resolution around 1µm [6]. With such a high resolution FFOCT systems can produce images that are similar to that obtained with classical histology procedures and can thus be important tools for pathology [7,8]. This is why we worked on combining the interest of a setup with a needle probe with the performances of FFOCT. We will first present the principle and performances of our endoscopic FFOCT setup, and then show *ex vivo* and *in vivo* imaging results.

2. Instrument and method for *in situ* optical biopsy

2.1. Experimental setup

Full-field OCT endoscopic setups have already been proposed by other groups [9,10]. The main principle of such systems is presented on Fig. 1. It is based on the coupling of two distinct interferometers: one is external to the probe, and one is placed at the distal end of the probe in contact with the tissue to image, as proposed in [11].

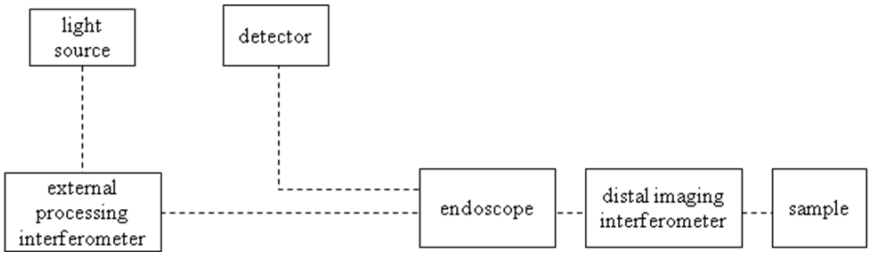

Fig. 1. Principle of a full-field OCT system with two coupled interferometers.

#150895 - $15.00 USD Received 11 Jul 2011; accepted 23 Jul 2011; published 29 Sep 2011

Indeed an endoscopic full-field OCT system with only one interferometer would require to set identical probes in both arms of the Linnik interferometer [12], which would induce very large optical path lengths. On the contrary, in a system with two interferometers the probe is not part of an interferometer arm and is only used to transport an image. It is thus entirely passive and insensitive to its environment. Such a system is to privilege for *in situ* imaging, where one needs a system able to image outer or inner parts of the body that are difficult to reach.

However, to the best of our knowledge, previously described endoscopic full-field OCT setups did not succeed in demonstrating a system suitable for both *in situ* and *in vivo* biomedical endoscopic imaging. A first system used a spatially and temporally incoherent light source, an external Michelson interferometer, a distal Linnik interferometer at the end of an optical fiber, and a fiber bundle for 2-D image collection [9]. It demonstrated a good ability to image biological samples but the use of a complete Linnik interferometer or other bulk interferometers at the distal end of the probe does not allow for *in situ* endoscopic imaging mainly because of its size. A second system used a spatially coherent and temporally incoherent light source, a fiber bundle-based probe used both for illumination and recollection, and a common-path interferometer at the end of the bundle [10,13]. The simple miniaturized probe is suitable for endoscopy but the system demonstrates a low sensitivity, typically −60 dB, which does not allow imaging of biological tissues.

In our system we decided to use a source with very low temporal and spatial coherence. Indeed the temporal incoherence ensures a good axial resolution, whereas the spatial incoherence increases the sensitivity by decreasing cross-talk effects. Moreover we also use a very simple common-path distal interferometer. The advantage compared to scanning system [14] is that it does not require any advanced miniaturized mechanical systems at the tip of the probe, which are likely to increase the diameter as well as the cost of the probe. Our simple design is well-suited for *in situ* imaging.

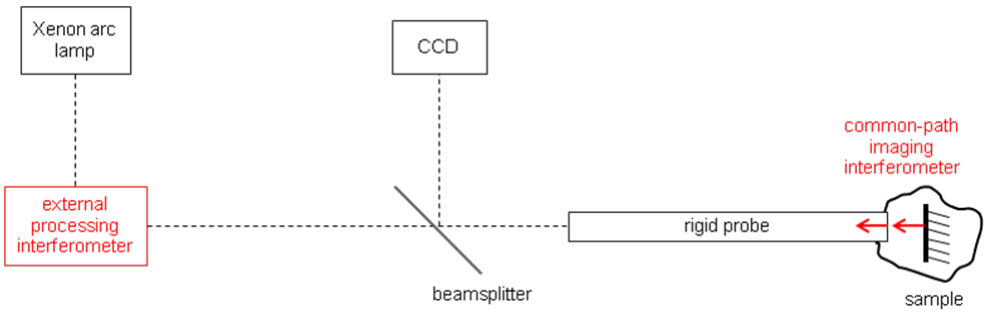

Fig. 2. Simplified principle of our full-field OCT system with a common-path imaging interferometer (focusing and conjugating optics are not shown).

The principle of our system is described on Fig. 2. We use a broadband white light source such as a Xenon arc lamp coupled to an optical fiber. This source spectrum is not as smooth as the one obtained with a thermal light source, e.g. a tungsten filament, but the luminance and the power level injected into the fiber are much higher. It illuminates a Michelson-type processing interferometer, which modulates the spectrum at a frequency dependent on the path length difference. This spectrum is then injected into the probe to the distal imaging interferometer. We chose it to be common-path: interferences occur between the reference beam reflected at the tip of the probe and light backscattered by structures at each depth within the tissue. The 2-D detector, a 1 mega-pixel camera such as a CCD (Dalsa M60) or CMOS (Photonfocus), detects the superposition of the modulated spectra coming from the processing interferometer and from the imaging interferometer. A maximum signal is detected only when both path length differences match, so that by setting the path length difference of the external interferometer one sets the imaging depth within the sample. Figure 3 shows for example the signal collected from a planar mirror as a function of the path length difference

#150895 - $15.00 USD Received 11 Jul 2011; accepted 23 Jul 2011; published 29 Sep 2011

mismatch between both interferometers. Furthermore, for extracting the interference signal from the background we use a phase shifting method with a piezoelectric modulation in the processing interferometer [15]. A 3D image can be reconstructed by performing a one-dimensional depth scan using the processing interferometer.

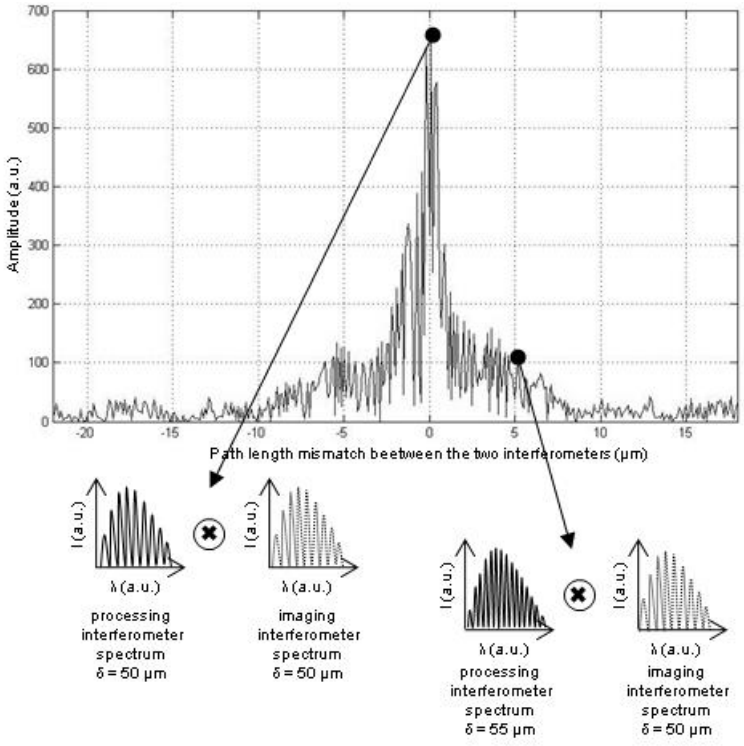

Fig. 3. Signal collected on one point of the 2-D detector showing interference fringes coming from a planar mirror placed at 25 µm ahead of the probe in air. The path length difference of the imaging interferometer is thus 50 µm. The path length difference of the external interferometer is scanned from 30 to 70 µm using a step motor.

2.2. Performances

Our system can be used with different probes without changing the bulk setup. The following results were obtained with a rigid probe based on a Graded-Refractive-INdex (GRIN) lens assembly with a diameter of 2 mm and a length of 150 mm (GRINTECH, Germany).

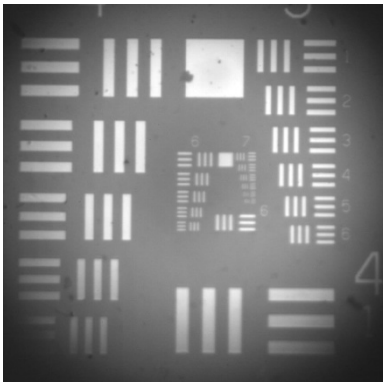

Fig. 4. Direct image of a 1951 USAF target.

#150895 - $15.00 USD Received 11 Jul 2011; accepted 23 Jul 2011; published 29 Sep 2011

The transverse resolution of the system depends on the probe optics. To measure it we image a 1951 USAF target as shown on Fig. 4. Using the FWHM of the first derivative of the edge response function it was calculated to be 3.5 µm in air. The axial resolution depends directly on the coherence length of the light source; by measuring the FWHM of the fringe envelope it was found to be 1.8 µm in water. Sensitivity was experimentally evaluated using a partial reflector with −33 dB reflectivity. A value of −80 dB was obtained when averaging 20 images during about 1 second, which should be enough to get signal from biological tissues.

2.3. Proof of principle on a phantom

First experiments with this setup were conducted as a proof of principle on a phantom made of polyurethane with micrometer-scale TiO_2 beads. Figure 5 shows an image of the phantom at a depth of 100 µm. We can clearly distinguish each individual bead as well as clusters of beads.

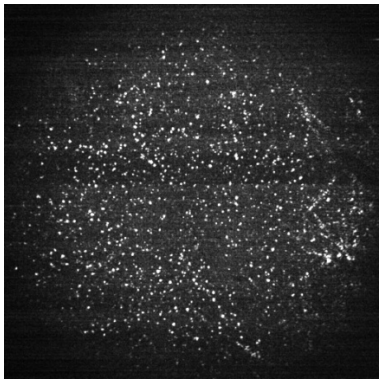

Fig. 5. En face image of a polyurethane phantom with TiO_2 beads acquired with our setup at a depth of 100 µm. Field of view is 1.5 mm x 1.5 mm.

3. *Ex vivo* study on human breast tissue

3.1. Method and results

Fixed unstained human breast tissue samples were covered in water-based gel (Ultrasonic) and the probe was directly applied in contact with each sample. Although it is not mandatory, the use of an index-matching medium is often useful to ensure a complete contact between the probe and the sample when the sample surface is rough. Indeed the presence of residual air

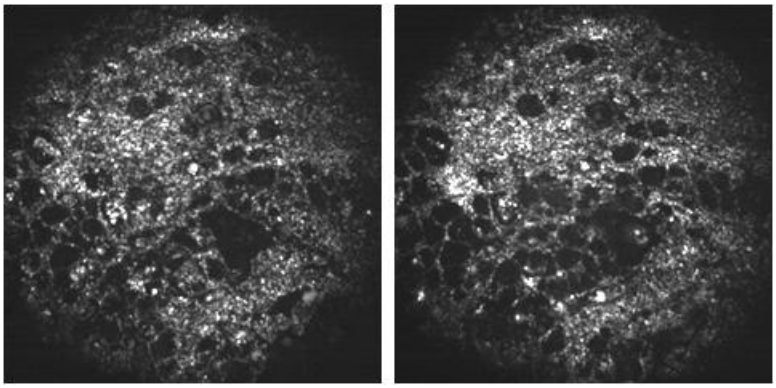

Fig. 6. En face images of fixed human breast tissue at depths of 20 µm and 30 µm. Field of view is 1.5 mm x 1.5 mm.

#150895 - $15.00 USD Received 11 Jul 2011; accepted 23 Jul 2011; published 29 Sep 2011

bubbles would create strong backreflections at the interface and thus degrade image quality. Instead of the water-based gel we could however have used other media such as water or saline. Examples of imaging results are presented on Fig. 6. We can see strong backscattering connective tissue as well as adipocytes easily recognizable as black round-shaped cells.

3.2. Comparison with classical FFOCT images

We compared images obtained with our setup with images obtained on a classical non endoscopic FFOCT system (Light-CT^{TM} scanner from LLTech, France). Figure 7 shows images taken on two different areas of a human breast tissue sample.

As we expected we obtain images of lesser quality: the endoscopic setup has a lower sensitivity but also a three times lower lateral resolution, due to the choice of the probe optics. Indeed the coherence plane of our setup can be scanned with the processing interferometer but the focal plane stays fixed. That is why we have chosen a probe with a relatively low NA, 0.1, in order to have a larger depth of field, so that we can typically image up to 100 µm in depth. In comparison the Light-CT^{TM} scanner uses microscope objectives with a higher N.A. of 0.3. The different structures of the tissue can all the same be identified in both images: hypo-scattering fat cells and hyper-scattering fibered connective tissue.

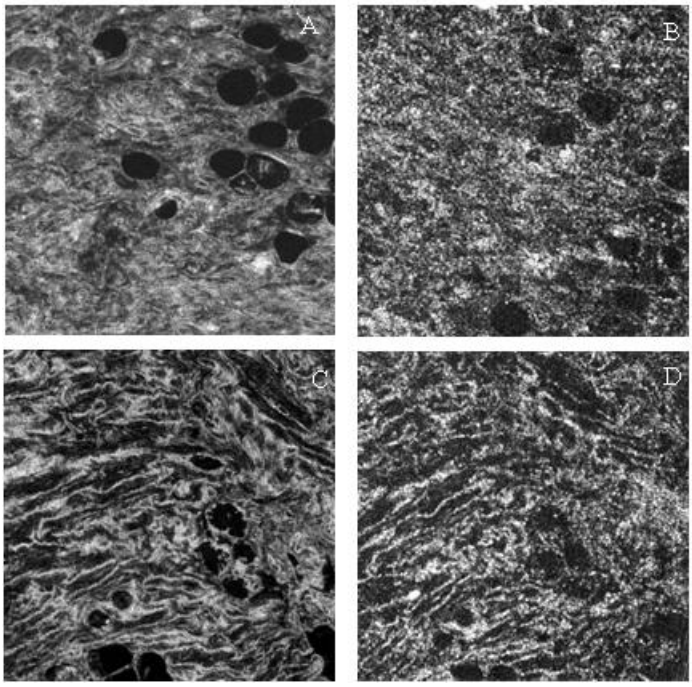

Fig. 7. En face images of fixed human breast tissue at depth 40 µm on two different areas (upper images and lower images). (A) & (C): classical FFOCT images. (B) & (D): corresponding endoscopic FFOCT images. Field of view is 1 mm x 1 mm.

4. Preliminary *in vivo* study on human skin

4.1. Motion artifacts

A main difficulty of *in vivo* imaging is to stabilize the tissue in order to avoid motion artifacts. In previous studies using confocal microscopy [16] or OCT [17] a fixture ring is placed on the area to image with or without adding adhesive. The area is covered with an index-matching medium and a cover glass window is then pressed on the tissue. This technique allows capturing good-quality images at a given depth, but not in-depth stack images in the same field. For our study we covered the tissue with index-matching water-based gel, placed the tip

#150895 - $15.00 USD Received 11 Jul 2011; accepted 23 Jul 2011; published 29 Sep 2011

of the probe directly in contact with the tissue and applied a light pressure. This ensured a sufficient stabilization of the tissue for imaging at short depths, up to a few hundred microns.

4.2. Results

We acquired images on human skin, lip and forearm of a healthy volunteer. For this preliminary study we did not use any clearing agents, although other groups have previously demonstrated that it could quite enhance the quality of images and increase depth penetration of light [18]. Images taken on the lower lip are presented on Fig. 8. They show large-scale structures of the tissue as well as fine details such as epithelial cells.

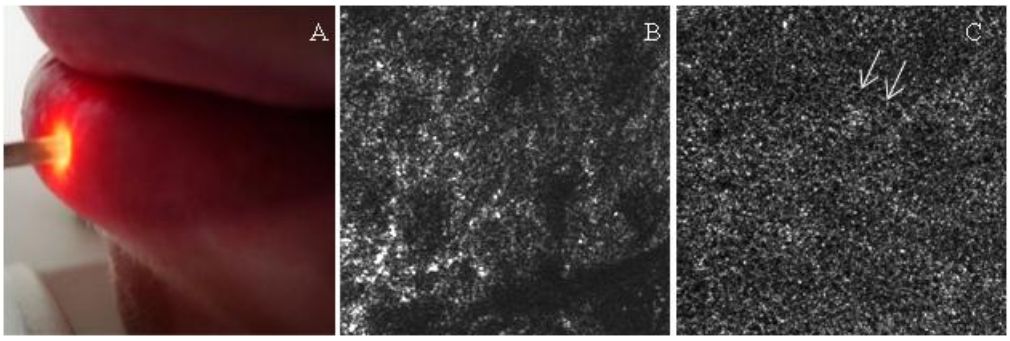

Fig. 8. En face images of *in vivo* human lip. The probe is placed directly in contact with the tissue (A). Lip tissue at 20 µm under the surface showing wrinkles (B) and lip tissue at 60 µm under the surface showing a pattern of epithelial cells (arrows) (C). Field of view is 1 mm x 1 mm.

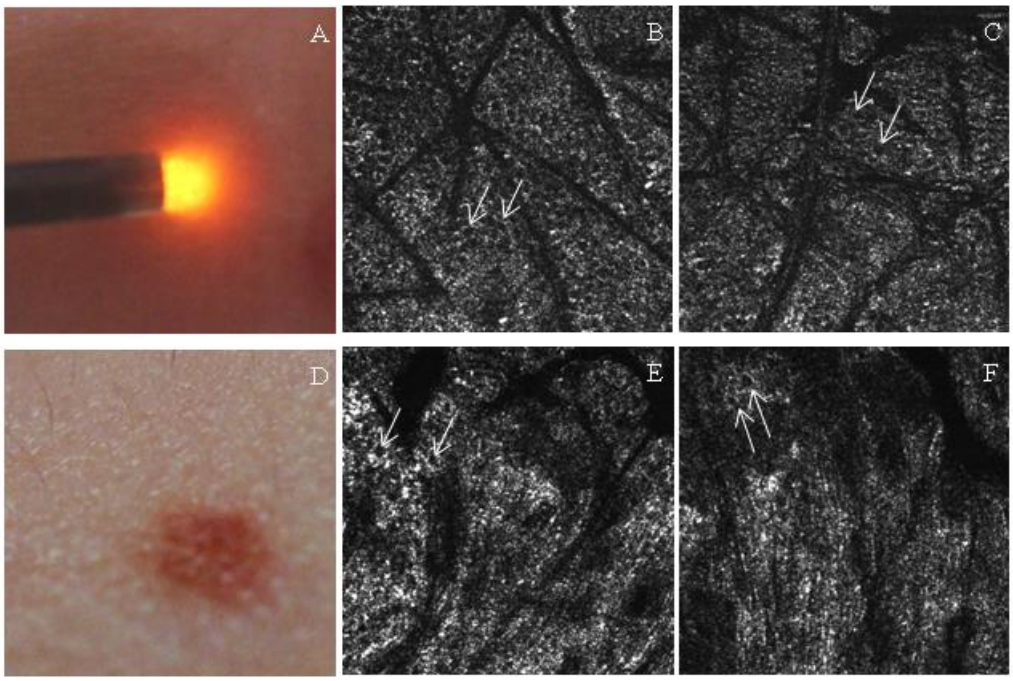

Fig. 9. En face images of *in vivo* human skin. (A) The probe is applied on forearm tissue: healthy tissue at 20 µm under the surface (B) (C) showing wrinkles and epithelial cells (arrows). (C) The probe is applied on a mole: mole tissue at 20 µm under the surface (E) (F) showing only a few epithelial cells (arrows) and long fibered structures. Field of view is 1 mm x 1 mm.

#150895 - $15.00 USD Received 11 Jul 2011; accepted 23 Jul 2011; published 29 Sep 2011

Figure 9 shows results obtained on normal forearm skin and on a mole, at depths around 20 µm. Normal tissue exhibits wrinkles, which have a typical depth of 100 µm and a width between 20 and 50 µm, and regular epithelial cells with a typical diameter of 30 µm. Structures are totally different on mole tissue: only a few epithelial cells are present, and the tissue exhibits large-scale fibered structures.

5. Discussion and conclusion

To summarize, our setup has proven its ability to image biological tissues *ex vivo* and reveal fine tissue structures thanks to its micrometer-scale resolution. Preliminary *in vivo* experiments on skin give promising results. The design of our probe, allowing diameters ranging from less than 1 mm to a few mm, makes it suitable for *in situ* imaging of different accessible areas.

However several points still have to be improved for future development of a medical device. In this work the acquisition time of one 2-D image was typically 1 second, but we plan on reaching a frequency of several Hz. This can be done by acquiring a more powerful light source and a faster 2-D camera, and by improving the mechanical setup to increase the sensitivity of the system, thus reducing the number of accumulations needed to have a good image quality. Another limitation of our current setup is that although the imaging depth can be easily scanned through the tissue, the focal depth stays fixed at a given depth. The imaging range is therefore limited by the depth field of the probe optics. Since it is typically 50 µm we were only able to image tissues up to depths around 100 µm. However we could introduce dynamic focusing relatively easily thanks to the use of GRIN lenses. Indeed one can displace the focal plane at the exit of a GRIN lens by displacing the focal plane at the entrance, for example using a microscope objective or lens system mounted on a linear motor. Such a system has already been previously described by other groups [19]. Finally, the current bulk setup has to be designed into a hand-held probe in order to be able to access areas of interest on the patient's body. A hand-held probe could then be used in dermatology for imaging of the skin, but it could also guide the surgeon during tumor removal operations and guide biopsy procedures, for example in the breast.

In the meantime this system could also be implemented with a flexible probe based on a fiber bundle. In comparison with the rigid probe the image quality would be degraded due to the pixelation effect of the fibers, but a system with a flexible probe would allow for imaging of areas inaccessible with the rigid probe. It could for instance be used in the aero-digestive and gastrointestinal tracts.

We believe *in vivo* and *in situ* applications of FFOCT for endoscopic evaluation could be very crucial for the clinician and the surgeon. It could allow the clinician to better evaluate the nature of the lesion he has discovered and to choose the field of mucosa he has to biopsy for conventional morphologic diagnosis or ancillary diagnosis techniques in the screening of bronchus cancer as well as colon or gastric cancer, cervical uterus cancer, or vesicle cancer. Also during coelioscopy or thoracoscopy for example, the surgeon has not the ability to palpate directly with the hand the tissue and to appreciate the induration related to an eventful neoplasm. Our minimally invasive technique could improve the appreciation of the surgeon.

Acknowledgments

We would like to thank Fabrice Harms, Franck Martins, Charles Brossollet and Sophie Angogna, members of the LLTech company, Paris (France), for technical support and advice, and the Institut Curie, Paris (France), for providing the excised samples.